Dear Editor and Anonymous Reviewer:

We greatly appreciate reviewer's insightful and helpful comments regarding our manuscript. The manuscript has been revised based on reviewer's comments. Following the reviewers' suggestions, the revised manuscript provides a more detailed description based on the theories of Reichl and Deike (2020) as well as the $dpCO_2$-driven negative feedback mechanism and carbonate–pH system adjustment associated with ocean buffering effects, consistent with the findings of Rustogi et al. (2025).

In addition, we moved the descriptions of the model framework, experiments, and POP2–waves coupling methodology to the beginning of Section 2, while the introduction of the model validation data was moved to the end of Section 2. This restructuring provides a more direct and coherent presentation of the model framework. The reworded results are presented alongside the relevant figures and discussed within a broader scientific context. Below are the point-by-point replies to reviewer's comments and concerns.

Sincerely,
Yung-Yao Lan, Huang-Hsiung Hsu, Wei-Liang Lee and Simon Chou

Anonymous Referee #2
The reviewer comments are formatted in italics and the authors response to the comments are formatted in bold.
Notation *RC2.P#* represents Reviewers Comment. Paragraph Number

Specific comments:

RC2.1 L26/Figure 9: The interpretation of the regressions should consider the flux direction. The sign convention in this paper assumes that ocean outgassing is positive, so it's positively correlated with kw, while ocean uptake is negatively correlated with kw; however, its magnitude may still be enhanced, if not more so. Consider providing more interpretation than simply stating correlations. For example, kw and SST are negatively correlated because they reflect the latitudinal structure of colder ocean waters and more intense sea states.

Response:

To confirm the statistical significance of the variables, we first conducted a t-test (at the 95% confidence level). Subsequently, we standardized both the air–sea CO_2 flux and the relevant variables (air–sea $dpCO_2$ (Fig. 9a), $K_{w,660}$ (Fig. 9b), SST (Fig. 9c), and pH (Fig. 9d)) into anomalies with a mean of 0 and a standard deviation of 1, thereby removing the influence of differing units and enabling comparison on a common scale. This allows the LRC to range between −1 and +1.

In the revised manuscript, we have added the following explanation to clarify the relationship between air–sea CO_2 flux and sea state: $K_{w,660}$ and SST are negatively correlated, reflecting the latitudinal gradient where colder, high-latitude waters are associated with more intense sea states and higher $K_{w,660}$. This pattern occurs because lower temperatures in high-latitude regions increase CO_2

solubility, thereby enhancing oceanic uptake. Conversely, higher temperatures in tropical regions reduce solubility, promoting CO_2 outgassing. As SST increases, CO_2 molecules become more mobile in seawater, enhancing diffusion and reducing the Schmidt number (Sc=ν/D, the ratio of kinematic viscosity to the diffusion coefficient). Because K_w is parameterized as $Sc^{-0.5}$, a decrease in Sc leads to an increase in $K_{w,660}$ and air–sea CO_2 flux.

RC2.2 L37: Consider adding a line that makes the flux direction convection explicit, clearly stating that positive fluxes are ocean outgassing to the atmosphere.

Response:

Thank you for your suggestion. Please see the revised manuscript for the change.

RC2.3. L44/L139/L230: I believe the equation you're showing is from Wanninkhof (2014), not from Wanninkhof (1992). Please modify here and elsewhere. Please add that the 10 m wind speed is the neutral wind speed.

Response:

Thank you for pointing out the mistake. In the B-CTL control experiment, the coefficient (k) for gas transfer velocity in Equation (2) follows Wanninkhof (1992), where k = 0.31. I mistakenly entered 0.251, which may have led to confusion with Wanninkhof (2014); this has now been corrected in the revised manuscript. For further details, please refer to the original CESM1 POP2 code (ecosys_mod.F90), specifically the annotation of the variable *xkw_coeff* (! a = 0.31 cm/hr s^2/m^2 in (s/cm)) and Table RC1.1.

In the revised manuscript, Eq. (2) includes an additional symbol description: U_{10}^2 represents the squared neutral mean wind speed at 10 m above the surface.

Table RC1.1 The coefficient (k) used to parameterize gas transfer velocity ($K_{w,660}$) differs between Wanninkhof (1992) and Wanninkhof (2014).

	Wanninkhof (1992)	Wanninkhof (2014)
the coefficient (k) of gas transfer velocity ($K_{w,660}$) $K_{w,660} = k <U_{10}^2> (Sc/660)^{-0.5}$	0.31	0.251
optimal method	applicable to deduce $K_{w,660}$ at steady winds	The optimal coefficient was obtained using an inverse

		modeling approach with CCMP[1] winds and the Modular Ocean Model General Circulation Model (MOM3 GCM).

Note:[1]CCMP: The Cross-Calibrated Multi-Platform (CCMP) are produced by Remote Sensing Systems (RSS) with support from a NASA Ocean Vector Winds Science Team grant.

RC2.4. Rustogi et al. (2025) used an ocean circulation model to quantify wave-bubble effects on CO2. Might be a relevant reference.

Response:

We thank the reviewer for the helpful suggestion to better clarify the model framework. Rustogi et al. (2025) employs a fully coupled ocean–biogeochemistry modeling system based on the MOM6 ocean circulation model and the COBALTv2 biogeochemical module. This framework simulates ocean dynamics, temperature, and carbon cycling processes including dissolved inorganic carbon (DIC), pCO_2, and wave effects in the air–sea CO_2 exchange. They also describe a nonlinear pCO_2 feedback mechanism within the coupled ocean–carbon system that regulates air–sea CO_2 flux.

Rustogi et al. (2025) also indicate that as pCO_2^w responds to changes in DIC and alkalinity, the air–sea $dpCO_2$ is partially reduced. This induces a negative feedback loop, whereby enhanced CO_2 uptake (or outgassing) is damped by chemical re-equilibration within the marine carbonate system, consistent with the findings of this study. Furthermore, Wu et al. (2025) also investigated the influence of these mechanisms within a global ocean coupled model, aiming to better capture the indirect effects of changes in surface DIC—driven by air–sea CO_2 flux—on the flux itself.

Reference

Rustogi, P., Resplandy, L., Liao, E., Reichl, B. G., and Deike, L.: Influence of wave-induced variability on ocean carbon uptake. Global Biogeochem. Cy., 39, e2024GB008382. https://doi.org/10.1029/2024GB008382, 2025.

Wu, L., Cai, Y., and Rutgersson, A.: Ocean surface waves impact on global air-sea CO_2 flux, Biogeochem., 168, 68, https://doi.org/10.1007/s10533-025-01267-y, 2025.

RC2.5. Data, model experiments, and methodology: I agree with the other reviewer that there isn't sufficient information to understand how the model was spun up, how wave properties through coupling lead to the significant wave height variable, and about the individual model components, such as the biogeochemical module. Please also add information about how wind friction is calculated, as it's used in the wave-bubble formulation. Perhaps more details can be added to Figure 1, which is currently not very informative and, in its current form, should be moved to the supplementary material.

Response:

Thank you for your suggestion. We have substantially revised the methodology section of the manuscript, including (1) the development of the CESM1–POP2–waves model and its component modules (Sections 2.1 and 2.2), (2) a more detailed description of CarbonTracker (Section 2.3), (3) additional information on POP2–waves input data and atmospheric forcing (Sections 2.1 and 2.2), and (4) an expanded description of the Marine Biogeochemistry (MARBL) module in Section 2.1 and Fig. 1, highlighting that all components influence the air–sea CO_2 flux. Please refer to the revised manuscript for details of these changes.

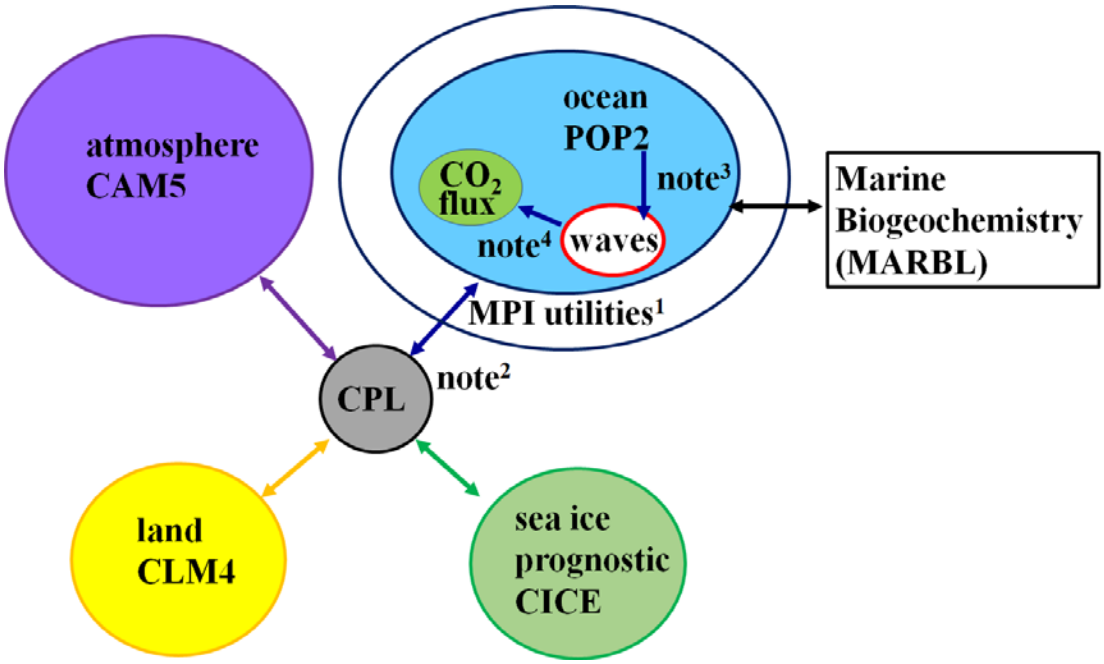

Figure 1. Architecture diagram for POP2–waves experiment in CESM1.2.2 framework, all components adhere to the CESM 1.2.2 framework, except for certain parts of the ocean component. The model components including components for the atmosphere [Community Atmosphere Model version 5 (CAM5)], land [Community Land Model version 4 (CLM4)], ocean [Parallel

Ocean Program, version 2 (POP2)], along with its associated modules—the waves module (waves) and the Marine Biogeochemistry (MARBL) module—sea ice [prognostic Los Alamos Sea Ice Model (CICE)], and the coupler (CPL).

Note:
[1]The wave-module variables are communicated between neighboring blocks via MPI, including zonal and meridional 10-m winds, wave radiation stress, subsurface momentum, and wave radiation and energy densities.
[2] To transfer variables such as zonal and meridional 10-m winds and friction velocity (including sea surface and ice fraction) from the CPL to POP2.
[3] The wave module receives variables from POP2, including the interpolation of depth-varying currents from z-coordinates (60 levels) to the wave module's vertical sigma coordinates (21 levels), along with ocean grid information in the x, y, and z directions.
[4] The wave module outputs significant wave height and friction velocity from the CPL for calculating the bubble-mediated gas transfer velocity in Eq. (3).

This study follows the NCAR CESM1 framework, in which the default friction velocity (u^*) is computed in the coupler (CPL) as part of the bulk aerodynamic formulation for air–sea momentum exchange. The friction velocity is derived from the surface wind stress and air density (Craig et al., 2012) as:

$$u^* = \sqrt{\frac{|\tau|}{\rho_a}}$$

Where τ is the surface wind stress vector (N m^{-2}) and ρ_a is the near-surface air density (kg m^{-3}). The magnitude of the wind stress (τ) is often parametrized as a function of wind speed at a 10-m height above the surface in the form:

$$\tau = \rho_a C_D u_{10}^2$$

Where ρ_a is the density of the surface air and C_D is a dimensionless wind drag coefficient which depends on atmospheric stability and surface roughness. In CESM1, the drag coefficient C_D is computed within the atmospheric boundary layer scheme (e.g., based on Monin–Obukhov similarity theory), and the resulting stress is passed through the coupler (CPL) to the ocean and sea ice components. Thus, the friction velocity used by ocean and wave-related parameterizations in CESM1 is dynamically consistent with the atmospheric forcing and surface exchange physics.

Reference

Craig, A. P., Vertenstein, M., and Jacob, R.: A new flexible coupler for Earth system modeling developed for CCSM4 and CESM1, Int. J. High Perform. Comput. Appl., 26(1), 31–42, doi:10.1177/1094342011428141, 2012.

RC2.6. L155: Equation 3 is missing a Schmidt term in the symmetric bubble gas exchange formulation. Please check the original publication. I'd suggest updating the formulation to the new generalized formulation proposed by Deike et al. (2025), which includes updated coefficients and an asymmetric bubble flux contribution, expected to have a small impact on CO2 but potentially significant for O2 fluxes.

Response:

We have added the Schmidt number term to the symmetric bubble gas exchange in Eq. (3). Deike et al. (2025) show that the wind–wave–bubble formulation explicitly decomposes gas exchange into nonbreaking, symmetric bubble, and asymmetric bubble components, introducing a physically based asymmetric bubble term that drives a unidirectional flux into the ocean independent of the air–sea dpCO_2. This framework emphasizes the process-level physics of bubble-mediated exchange and highlights the roles of gas solubility and bubble dynamics, particularly under energetic sea states.

We appreciate the suggestion to adopt this generalized formulation; however, implementing Deike et al. (2025) would require rerunning the simulations, which is not feasible at this stage as it would take more than one month to complete. As part of the ongoing development of a new biogeochemistry model within the CESM3 framework, we plan to implement the wind–wave–bubble parameterization of Deike et al. (2025). The updated model will be evaluated and compared with the present findings in a forthcoming manuscript.

RC2.7. L181/L184: These statements need more depth - what is consistent and what isn't? Perhaps adding global integrals values can help quantify if adding waves improves the match with the NOAA product. I agree with the other reviewer that adding difference plots may be more informative at least when comparing model simulations.

Response:

We further clarify the agreements and discrepancies in air–sea CO_2 flux among POP2-waves, B–CTL, and NOAA CT2022 in Section 3.1 and Figs. 3 and 4. The differences (B–CTL minus NOAA CT2022 and POP2-waves minus NOAA CT2022) are also shown in Fig. 2e–f. We do not use global integrals; instead, we analyze the 30-year monthly variability in the model simulations and the 20-year variability in NOAA CT2022, along with their standard deviations.

RC2.8. Figure 3: It isn't evident what this figure is demonstrating. The seasonal cycles vary between the product and coupled simulations across regions. If the point is to compare with the observation-based reference, then it's useful to continue that analysis throughout the manuscript; otherwise, it may be more informative to focus largely on the differences among the model simulations, since they are internally self-consistent. One interesting question would be to evaluate the difference in the carbon inventory in the ocean interior.

Response:

Thank you for your comment. Figure 3 presents the seasonal cycles of air–sea CO_2 flux, comparing product-based and coupled simulations across regions, as well as their differences relative to NOAA CT2022. The blue solid line represents NOAA CT2022, the black dashed line represents B–CTL, and the red solid line represents POP2–waves; the corresponding standard deviations are shown as bar graphs in the same colors.

Our experimental design focuses on air–sea carbon exchange at the interface, with limited output of broader carbon system variables. Ocean carbon inventory was not included in the initial design; however, it may be incorporated in future CESM3-based biogeochemical model development and experiment design.

RC2.9. Results: The results also include discussion material (e.g., L203-206, L282-283). In general, hard to understand the results without referencing the figures, and the text includes a lot of details about what the figures show, without interpreting the findings. Consider streamlining the key findings.

Response:

We have moved the discussion of Fay et al. (2024) to Section 4.2 and simplified the content in Lines 203–206 as follows. In the revised manuscript, the black dashed line and the red and blue solid lines represent the monthly means of B–CTL, POP2–waves, and NOAA CT2022, respectively, and the corresponding standard deviations are shown as bar graphs in the same colors.

We have revised the ambiguous wording in Lines 282–283 as follows. Johansson et al. (2022) reported that significant wave height generally increases with wind speed, but the relationship is strongly modulated by wind direction and regional conditions, leading to spatially variable and nonlinear wind–wave coupling.

Reference

Fay, A. R., Munro, D. R., McKinley, G. A., Pierrot, D., Sutherland, S. C., Sweeney, C., and Wanninkhof, R.: Updated climatological mean ΔfCO₂ and net sea–air CO₂ flux over the global open ocean regions, Earth Syst. Sci. Data, 16, 2123–2139, https://doi.org/10.5194/essd-16-2123-2024, 2024.

Johansson, M. M., Björkqvist, J.-V., Särkkä, J., Leijala, U., and Kahma, K. K.: Correlation of wind waves and sea level variations on the coast of the seasonally ice-covered Gulf of Finland, Nat. Hazards Earth Syst. Sci., 22, 813–829, https://doi.org/10.5194/nhess-22-813-2022, 2022.

RC2.10. Figure 5: The standard unit for kw is cm/hr - please update in this figure and elsewhere (Figure 7, L296). It isn't clear why the analysis shifts to focus on two regions (WP and EP) that weren't explicitly indicated by the masks in Figure 2.

Response:

We have converted $K_{w,660}$ to the standard unit (cm hr^{-1}) in Figs. 5 and 7 and in Line 296. Xu et al. (2022) indicate that, in CMIP6 models, the Atlantic Ocean exhibits regionally varying SST biases arising from both dynamical and thermodynamical limitations, while the Southern Ocean shows a persistent warm bias, a well-known issue in many Earth system models. We exclude these regions to focus on how strong wave effects influence $K_{w,660}$ and air–sea CO_2 exchange in areas with the most pronounced positive or negative fluxes. The WP region (160–180°E, 35–40°N) exhibits the strongest negative air–sea CO_2 flux within the NWP (Fig. 2d), whereas the EP region (230–250°E, 0–5°S) within the EEP (Fig. 2d) exhibits the strongest positive air–sea CO_2 flux. Table RC2.10.1 provides a comparison of the corresponding mean air–sea CO_2 flux values.

Table RC2.10.1 Mean air–sea CO_2 fluxes in regions with the most pronounced positive and negative values (mol m^{-2} yr^{-1}).

Positive air–sea CO_2 fluxes		**Negative air–sea CO_2 fluxes**	
EP (230–250°E, 0–5°S)	**EEP in Fig. 2d**	**WP (160–180°E, 35–40°N)**	**NWP in Fig. 2d**
3.7	**1.8**	**-3.9**	**-3.0**

Reference

Xu, G., Chang, P., Ramachandran, S., Danabasoglu, G., Yeager, S.,

Small, J., Zhang, Q., Jing, Z., and Wu, L.: Impacts of Model Horizontal Resolution on Mean Sea Surface Temperature Biases in the Community Earth System Model, J. Geophys. Res.-Oceans, 127, e2022JC019065, https://doi.org/10.1029/2022JC019065, 2022.

RC2.11. Figure 6: Consider adding wind speed distribution to better distinguish modeled responses.

Response:

In Fig. 6, we examine the relationship between air–sea CO_2 flux and U_{10} under high-wind conditions (U10 > 10 m s^{-1}) in the Western Pacific (160–180°E, 35–40°N), with regression lines shown for (a) B–CTL and (b) POP2–waves. As indicated in Fig. 5a, there is a significant difference in $K_{w,660}$ between POP2–waves and B–CTL under U_{10} > 10 m s^{-1} in this region. The x-axis in Fig. 6 shows the wind speed distribution. Overall, U_{10} and the negative air–sea CO_2 flux exhibit a linear relationship, with a stronger correlation in POP2–waves (R=0.48) than in B–CTL (R=0.35), indicating that the wave-related $K_{w,660}$ under high-wind conditions better captures air–sea CO_2 flux variability in this region.

.

RC2.12. Figure 7: The figure doesn't show the surface circulation or the Hs fields as stated in the text. The Kw from the ctrl experiment and the kwNB from the wave experiment aren't directly comparable, so if the point is to compare the two, it should be the total kw, and perhaps their difference. Could you comment on the kw pattern in panel c: it lacks the structure seen across products and modeled fluxes (e.g., Reichl and Deike, 2020) – is it related to the coupling? Are there other references that demonstrate that the kw/flux structure is CESM-specific?

Response:

Thank you for pointing out the mistake. In Fig. 7a, the shaded areas represent the near-surface atmospheric condition of 10-m wind speed (U_{10}, m s^{-1}), with contours indicating sea level pressure (PSL, mb). Figure 7b shows the H_s fields with contours, as described in Lines 283–286 of the original manuscript. This clarifies the relationship between the H_s fields and the ratio of $K_{wB,660}$ to $K_{w,660}$ described in the text.

We changed the contours in Fig. 7d to represent the difference ($K_{wNB,660}$−$K_{wB,660}$) in cm hr^{-1}, illustrating the difference in gas transfer velocity between the non-bubble ($K_{wNB,660}$) and bubble ($K_{wB,660}$) components under different spatial distributions of u^* (Fig. 7b) and U_{10} (Fig. 7a).

Since the percentage ratio of $K_{w,660}$ ((POP2–waves−B–CTL)/B–CTL) is unclear and does not adequately represent the magnitude of the difference between POP2–waves and B–CTL, we changed the contours in Fig. 7c to show the absolute difference in $K_{w,660}$ (POP2–waves − B–CTL) in cm hr^{-1}.

Figure 7c shows that the larger differences in $K_{w,660}$ (POP2–waves − B–CTL) are mainly distributed in regions with higher H_s, particularly within 30°N–30°S. Although wind speeds in the Indian Ocean and tropical Pacific are relatively low (< 5 m s^{-1}; Fig. 7a), the $K_{w,660}$ values in POP2–waves are still about 9 cm hr^{-1} higher than those in B–CTL. In these regions, the POP2-waves enhanced $K_{w,660}$ is primarily dominated by the non-bubble-mediated component, as shown in Fig. 7d. Although H_s is also large in the Southern Ocean (Fig. 7b), it does not contribute substantially to the $K_{w,660}$ difference between POP2–waves and B–CTL because the high U_{10} in this region (Fig. 7a) already produces large $K_{w,660}$ values through the empirical formulation of Wanninkhof (1992).

Compared with Reichl and Deike (2020), this study presents the climatological U_{10} as shaded colors in Fig. 7a using a high-contrast color bar, showing patterns similar to those in Fig. 1d of Reichl and Deike (2020), despite their use of a single-color scale. This study also presents climatological H_s contours in Fig. 7b, which are similar to those shown in Fig. 1e of Reichl and Deike (2020). Both studies exhibit common features, with high U_{10} and H_s values distributed over the North Pacific around 30°–50°N, the Indian Ocean around 10°–20°S, and the Southern Ocean. Because $K_{w,660}$ is strongly influenced by both U_{10} and H_s, the spatial distribution of B–CTL $K_{w,660}$ (shaded) and the contours difference $K_{w,660}$ (POP2–waves − B–CTL) shown in Fig. 7c is also similar to Fig. 1f of Reichl and Deike (2020), which indicated in Fig. RC2.12.1.

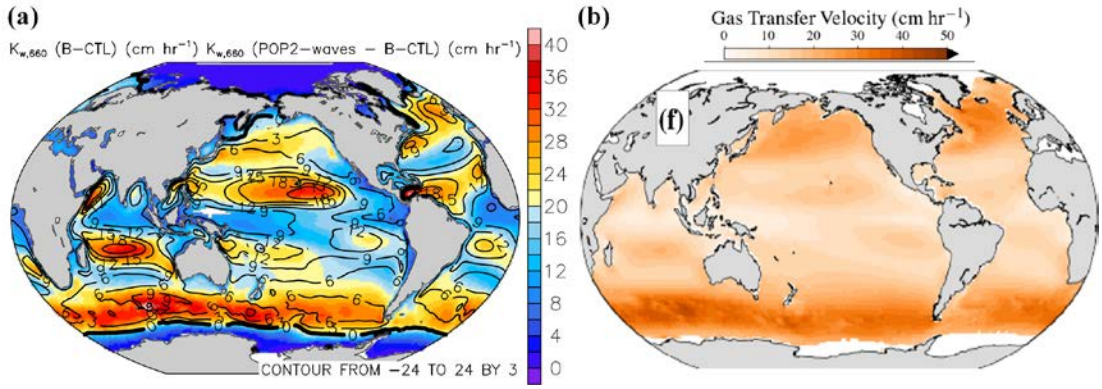

RC2.12.1. Comparison of $K_{w,660}$ between this study and Reichl and Deike (2020):

(a) Fig. 7c in this manuscript and (b) Fig. 1f in Reichl and Deike (2020).

RC2.13. L290: There shouldn't be a discrepancy in the Ab coefficient between this study and Reichl and Deike's formulation, since that's what is used here. Perhaps the differences have more to do with the tool?

Response:

Yes, the A_B coefficients follow the formulation suggested by Reichl and Deike (2020). The ratio of $K_{wB,660}/K_{w,660}$ in POP2–waves can be expressed as follows:

$$\frac{K_{wB,660}}{K_{w,660}} = \frac{\frac{A_B}{K_0\,R\,T_0}u_*^{\frac{5}{3}}(g\,H_S)^{\frac{2}{3}}\left(\frac{Sc}{660}\right)^{-\frac{1}{2}}}{A_{NB}u_*\left(\frac{Sc}{660}\right)^{-\frac{1}{2}}+\frac{A_B}{K_0\,R\,T_0}u_*^{\frac{5}{3}}(g\,H_S)^{\frac{2}{3}}\left(\frac{Sc}{660}\right)^{-\frac{1}{2}}} \qquad \text{(RC2.13.1)}$$

When the Schmidt number term is removed, the ratio of $K_{wB,660}/K_{w,660}$ can be expressed as follows:

$$\frac{K_{wB,660}}{K_{w,660}} = \frac{\frac{A_B}{K_0\,R\,T_0}u_*^{\frac{5}{3}}(g\,H_S)^{\frac{2}{3}}}{A_{NB}u_*+\frac{A_B}{K_0\,R\,T_0}u_*^{\frac{5}{3}}(g\,H_S)^{\frac{2}{3}}} \qquad \text{(RC2.13.2)}$$

Compared with Reichl and Deike (2020), the constant coefficients are the same; therefore, after substituting the numerical values of A_{NB} (1.55 ×10^{-4}, no dimension), A_B (1.2 ×10^{-5} s^2 m^{-2}), R (0.082 L atm mol^{-1} K^{-1}), and g (9.806 m s^{-1}) and simplifying, the ratio $K_{wB,660}/K_{w,660}$ can be expressed as follows:

$$\frac{K_{wB,660}}{K_{w,660}} \propto \frac{4.32\frac{1}{K_0\,T_0}u_*^{\frac{5}{3}}(H_S)^{\frac{2}{3}}}{u_*+4.32\frac{1}{K_0\,T_0}u_*^{\frac{5}{3}}(H_S)^{\frac{2}{3}}} \propto \frac{4.32\frac{(u_*H_S)^{\frac{2}{3}}}{K_0\,T_0}}{1+4.32\frac{(u_*H_S)^{\frac{2}{3}}}{K_0\,T_0}} \qquad \text{(RC2.13.3)}$$

The main difference in the ratio $K_{wB,660}/K_{w,660}$ between Reichl and Deike, (2022) and this study lies in $\frac{(u_*H_S)^{\frac{2}{3}}}{K_0\,T_0}$. Table RC2.13.1 summarizes the differences in the sources of the parameters used in Eq. RC2.13.3.

Table RC2.13.1 The differences in the sources of the parameters between Reichl and Deike, (2020) and POP2-waves

item	Reichl and Deike, (2020)	POP2-waves (this study)
T_0 (SST)	**T_0 derived from satellite observations**	**T_0 is obtained from POP2 simulations**
***H_s* (significant wave height)**	***H_s* simulated with WAVEWATCH III**	***H_s* is generated by the POM wave module coupled within the POP2 system**
***k_0* (solubility constant)**	**The empirical relationship of Weiss (1974)**	**The empirical relationship of Weiss (1974)**
u* (friction velocity)	**u* estimated from U_{10} using the bulk parameterization of**	**u* is computed in the coupler as part of the bulk**

	Edson et al, (2013)	**aerodynamic formulation for air–sea momentum exchange**

Since the sources of the $K_{w,660}$ parameters (T_0, H_s, and u*) differ substantially, the spatiotemporal distribution of $\frac{(u_* H_S)^{\frac{2}{3}}}{K_0\ T_0}$ also differs between Reichl and Deike, (2020) and this study. The bubble contribution to the total gas transfer velocity ($K_{wB,660}/K_{w,660}$) in POP2–waves is approximately 38%, which is slightly higher than ~30% reported by Reichl and Deike (2020).

Reference

Edson, J. B., Jampana, V.,Weller, R. A., Bigorre, S. P., Plueddemann, A. J., Fairall, C.W., Miller, S. D., Mahrt, L., Vickers, D., and Hersbach, H.: On the exchange of momentum over the open ocean. J. Phys. Oceanogr., 43, 1589 – 1610, https://doi.org/10.1175/JPO-D-12-0173.1, 2013.

RC2.14. L310: This point is not sufficiently demonstrated in your study - there is only a brief mention of changes in pH in two ocean regions. Either remove or restructure results to show this.

Response:

We removed the description in L310–315 and restructured the results after introducing the marine carbonate system related to pH and total alkalinity in Section 4.1.

The marine carbonic acid system is a nonlinear, coupled system governed by CO_2 dissolution equilibrium, ($CO_{2(aq)} + H_2O \overset{K_H}{\leftrightarrow} H_2CO_{3(aq)}$), where the Henry's constant (K_H) for CO_2 in water at 25°C is approximately 3.4 x 10^{-2} (m/atm), two-step dissociation reactions, and the conservation of the total dissolved inorganic carbon (DIC) and total alkalinity (TA), ultimately determining pH and the distribution of carbonate species. The H_2CO_3 has two hydrogen ions and dissociates in two steps:

$H_2CO_3 \overset{K_{a1}}{\longleftrightarrow} H^+ + HCO_3^-$ **$K_{a1} = 4.4\times10^{-7}$** **(4, in manuscript)**

$HCO_3^- \overset{K_{a2}}{\longleftrightarrow} H^+ + CO_3^{2-}$ **$K_{a2} = 4.7\times10^{-11}$** **(5, in manuscript)**

The DIC can be expressed as

$$DIC = [H_2CO_3] + [HCO_3^-] + [CO_3^{2-}]$$

$$= K_H pCO_2^w + \frac{K_{a1} K_H pCO_2^w}{[H^+]} + \frac{K_{a1} K_{a2} K_H pCO_2^w}{[H^+]^2}$$

$$= K_H pCO_2^w \left(1 + \frac{K_{a1}}{[H^+]} + \frac{K_{a1} K_{a2}}{[H^+]^2}\right)$$

$$= K_H pCO_2^w ([H^+]^2 + K_{a1} [H^+] + K_{a1} K_{a2}) / [H^+]^2 \quad \textbf{(6, in manuscript)}$$

The marine carbonate system describes the distribution of DIC among its chemical species in seawater and is jointly governed by TA and pH. From Eq. (6), if the oceanic pCO_2^w and pH are known, the DIC can be determined, conversely, pCO_2^w can be inferred from DIC. TA is defined as the sum of the proton-neutralizing capacities of all weak acid anions in seawater (Dickson, 1981) and can be expressed as:

$TA=[HCO_3^-]+2[CO_3^{2-}]+[B(OH)_4^-]+[OH^-]+[HPO_4^{2-}]+2[PO_4^{3-}]+[SiO(OH)_3]+[NH_3]+[HS^-]-[H^+]-[H_3PO_4]$. In the POP2-waves framework, TA, pH and biogeochemistry are also used to calculate pCO_2^w.

When TA increases, the seawater becomes more alkaline, leading to an increase in CO_3^{2-} concentration and enhanced buffering of hydrogen ions. As a result, the $[H^+]$ decreases, causing pH to rise and increasing the ocean's capacity to absorb CO_2. Conversely, when TA decreases, the buffering capacity weakens, $[H^+]$ increases, pH decreases, and the ocean becomes more acidic with a reduced ability to uptake CO_2.

The biogeochemical module of POP2 (MARBL) updates TA in each grid cell by solving a coupled transport–reaction equation (Long et al., 2021). The average pH of the ocean is currently around 8.1 (Fig. 8c), reflecting slightly alkaline conditions. Within the DIC system, bicarbonate ions (HCO_3^-) are the dominant species because the prevailing pH lies between pK_{a1} and pK_{a2}. However, continued uptake of atmospheric CO_2 drives a decline in pH, a process termed ocean acidification. Our study highlights that wave-induced $K_{w,660}$ significantly influences the marine CO_2 system, altering alkalinity, pH, and carbonate speciation. These chemical changes, in turn, provide a feedback mechanism that modulates the overall dynamics of the air–sea CO_2 flux. In other words, perturbations in $K_{w,660}$ influence both $dpCO_2$ and air–sea CO_2 flux in the Earth System Model. This POP2–waves coupled behavior differs from traditional approaches that treat wave-induced $K_{w,660}$ and $dpCO_2$ as independent variables when estimating air–sea CO_2 flux (e.g., Reichl and Deike, 2020).

Reference

Long, M. C., Moore, J. K., Lindsay, K., Levy, M., Doney, S. C., Luo, J. Krumhardt, K. M., Letscher, R. T., Grover, M., and Sylvester, T.: Simulations with the marine biogeochemistry library (MARBL). J. Adv. Model. Earth Sy., 13(12), e2021MS002647. https://doi.org/10.1029/2021MS002647, 2021.

RC2.15. Discussion: There is nontrivial overlap between the discussion and the results. Consider rewording so the results are explained alongside the figures, while the discussion puts these results in a broader context.

Response:

We have eliminated redundant content throughout the manuscript; consequently, the results are presented alongside the relevant figures and discussed within a broader scientific context.

RC2.16. L343: The differences between simulations don't suggest mitigation or enhancement (which is a separate mechanism), just different mean states. Please reword.

Response:

The differences in pH between POP2–waves and B–CTL are not simply due to different mean states. Rustogi et al. (2025) indicate that faster equilibration of oceanic pCO_2 in the wind–wave–bubble simulation, driven by enhanced gas exchange, reduces the air–sea partial pressure difference. This pCO_2 feedback is strongest in the extratropics, where it suppresses CO_2 uptake. Our POP2–waves experiment shows a similar response, with increasing pCO_2 (Fig. 8b) and hydrogen ion concentration, accompanied by decreasing pH (Fig. 8d) in the extratropics. Because atmospheric CO_2 is fixed at 367 ppm in the B_2000_CAM5 compsets, the reduced $dpCO_2$ suppresses negative air–sea CO_2 flux referred to as negative feedback from $dpCO_2$. Rustogi et al. (2025) also showed that the effects of $\Delta K_{w,660}$ (between wave-induced and based on U_{10}) and $\Delta dpCO_2$ partially offset each other, although the $\Delta K_{w,660}$ effect is generally 20%–30% stronger than the counteracting $\Delta dpCO_2$ effect, explaining the modest increase in both positive and negative air–sea CO_2 fluxes in the wind–wave–bubble simulation.

Reference

Rustogi, P., Resplandy, L., Liao, E., Reichl, B. G., and Deike, L.: Influence of wave-induced variability on ocean carbon uptake. Global Biogeochem. Cy., 39, e2024GB008382. https://doi.org/10.1029/2024GB008382, 2025.

RC2.17. Section 4.3/Figure 10: The point about the negative feedback from pCO_2 is not explored enough - how was this feedback shut off in the simulations? Note that Rustogi et al. (2025) go into this in detail. This is a key difference between models and observation-based products.

Response:

Rustogi et al. (2025) show that although wave-enhanced $K_{w,660}$ increases local air–sea CO_2 exchange, the resulting rise in oceanic pCO_2 reduces the air–sea pCO_2 gradient in the extratropics, generating a carbonate chemistry feedback that partially offsets the increase in global ocean carbon storage. Furthermore, Rustogi et al. (2025) note that because observation-based products do not account for pCO_2 feedback, they may yield larger departures in global carbon sink estimates when accounting for wave-driven processes.

Section 4.3 and Fig. 10 fully present the large deviations in the global ocean carbon sink estimates caused by the absence of pCO_2 feedback when wave effects are considered. The manuscript Eq. 1 shows that air–sea CO_2 flux is determined by both $K_{w,660}$ and $dpCO_2$. In the B_2000_CAM5 compset, atmospheric CO_2 concentration is fixed at the year-2000 mean value (367 ppm), meaning that oceanic pCO_2 does not feedback to atmospheric CO_2 concentration or modify near-surface atmospheric and oceanic conditions. Therefore, POP2–waves and B–CTL share the same surface wind, temperature, and related physical forcing fields. Section 4.3 is thus designed as a virtual experiment. We did not recalculate the full set of biogeochemical variables in order to isolate the influence of carbon flux calculations between POP2–waves and B–CTL. Instead, we combined the air–sea $dpCO_2$ values from B–CTL with the wave-enhanced $K_{w,660}$ from POP2–waves, rather than explicitly calculating a fully coupled virtual air–sea CO_2 flux. This experimental design applies wave-induced $K_{w,660}$ without the accompanying $dpCO_2$-driven negative feedback, thereby introducing substantial uncertainty into the estimated air–sea CO_2 flux.

$$FCO_2 = K_{w,660} \cdot k_0 \cdot (pCO_2^w - pCO_2^a) \cdot (1 - ice) \qquad \textbf{(1, in manuscript)}$$

Yes, pCO_2-driven negative feedback is a key difference between coupled

models and observation-based products. Rustogi et al. (2025) highlighted that observation-based estimates, do not include pCO_2 feedback, which could potentially lead to larger deviations in global ocean carbon sink estimates when wave effects are considered.

Rustogi et al. (2025) demonstrate that while wave-enhanced $K_{w,660}$ accelerates local air–sea CO_2 exchange, it simultaneously reduces the air–sea $dpCO_2$. However, the magnitude of the air–sea CO_2 flux overestimation resulting from the lack of this $dpCO_2$-driven negative feedback has not been fully quantified in recent studies. The "lack of $dpCO_2$-driven negative feedback" case, which does not include real ocean buffering effects, allows positive air–sea CO_2 flux regions to release excess CO_2 into the atmosphere (> 0.4 mol m^{-2} yr^{-1}) while simultaneously enhancing excess CO_2 uptake (< −0.4 mol m^{-2} yr^{-1}) in negative air–sea CO_2 flux regions (Fig. 10b) compared to the coupled POP2–waves model.

Other points:

RC2.18. L9: Consider rewording this line — "Wave and bubble mechanisms impact the air-sea CO_2 flux by enhancing the gas transfer velocity (kw), often modeled through significant wave height (Hs)".

Response:

Thank you for your comment. We have reworded the sentence as follows: "Wave and bubble processes influence air–sea CO_2 flux by enhancing the gas transfer velocity (K_w), which is commonly parameterized as a function of significant wave height (H_s). Please see revised manuscript for the change."

RC2.19. L85: I agree with the other reviewer that if the point about data assimilation is to be included, it should be better motivated.

Response:

Thank you for your comment. We removed the description of a single data assimilation method for reconstructing air–sea CO_2 flux validation data in L87 and replaced it with the following statement: most validation datasets are derived from sparse ship-based pCO_2 observations combined with statistical interpolation, machine learning, atmospheric inversion, and climatological averaging to construct gridded long-term flux products. Please see revised manuscript for the change.

RC2.20. L92: Are you thinking of observation-based products when you reference non-model simulations? Please reword for clarity.

Response:

Yes, we refer to surface ocean observation-based products. Please see the revised manuscript for these changes.

RC2.21. Spell out acronyms WP and EP.

Response:

WP denotes the Western Pacific region (160–180°E, 35–40°N), and EP denotes the Equatorial Pacific region (230–250°E, 0–5°S). Please see the revised manuscript for these changes.